METHODS **25,** 19–30 (2001)
doi:10.1006/meth.2001.1212, available online at http://www.idealibrary.com on IDEAL®

Structural Dynamics of Catalytic RNA Highlighted by Fluorescence Resonance Energy Transfer

Nils G. Walter[1]

Department of Chemistry, University of Michigan, Ann Arbor, Michigan 48109-1055

RNA performs a multitude of essential cellular functions involving the maintenance, transfer, and processing of genetic information. The reason probably is twofold: (a) Life started as a prebiotic RNA World, in which RNA served as the genetic information carrier and catalyzed all chemical reactions required for its proliferation and (b) some of the RNA World functions were conserved throughout evolution because neither DNA nor protein is as adept in fulfilling them. A particular advantage of RNA is its high propensity to form alternative structures as required in subsequent steps of a reaction pathway. Here I describe fluorescence resonance energy transfer (FRET) as a method to monitor a crucial conformational transition on the reaction pathway of the hairpin ribozyme, a small catalytic RNA motif from a self-replicating plant virus satellite RNA and well-studied paradigm of RNA folding. Steady-state FRET measurements in solution allow one to measure the kinetics and requirements of docking of its two independently folding domains; time-resolved FRET reveals the relative thermodynamic stability of the undocked (extended, inactive) and docked (active) ribozyme conformations; while single-molecule FRET experiments will highlight the dynamics of RNA at the individual molecule level. Similar domain docking events are expected to be at the heart of many biological functions of RNA, and the described FRET techniques promise to be adaptable to most of the involved RNA systems.

RNA is a ubiquitous biopolymer. It constitutes 20% of the dry mass of *Escherichia coli*. RNA is involved in all aspects of the maintenance, transfer, and processing of genetic information. Only recently we have begun to fully understand the reason for this ubiquity: RNA has unique properties as a biomolecule, since it can serve a role in the coding and decoding (by specific Watson–Crick base pairing) as well as processing of genetic information (by forming intricately structured, often catalytically active components of the processing machinery (1)). The discovery of this dichotomy has fostered the idea of a prebiotic "RNA World," in which RNA was the sole genetic material that autocatalytically replicated in the absence of proteins, setting the stage for the development of life on earth (2). Apparently, some relics of this RNA World are conserved until the present day in the replication, transcription, splicing, editing, and translation machineries that feature RNA as an essential component.

While the ability to form Watson–Crick base pairs is a convincing reason for nucleic acids to store and read out genetic information up to the present day, it may be less obvious why RNA largely survived the continuous evolutionary challenge of protein enzymes to take over the catalytic role in the processing of genetic information. Two plausible reasons are given here. First, RNA can encode a biologically functional structure in a very short piece of genetic information. Examples are the "small" catalytic RNAs, or "ribozymes," that typically catalyze specific self-processing reactions in the rolling-circle replication of plant and animal viruses, viroids, or satellite RNAs (3, 4). One of the smallest naturally occurring RNA catalysts is the hairpin ribozyme, as derived from the satellite RNA of the tobacco ringspot virus (5); it is about 50 nucleotides in length, corresponding to 100 bits of genetic information. By comparison, a small protein catalyst of 90 amino acids is encoded by 270 nucleotides or 540 bits of genetic information. Second, RNA can undergo substantial structural rearrangements in the course of a reaction pathway without the need for an external energy source. Examples are again the hairpin ribozyme, which undergoes reversible transitions between open and closed conformations (6) that may well play a role

[1] To whom correspondence should be addressed. Fax: (734) 647-4865. E-mail: nwalter@umich.edu. Web site: http://www.umich.edu/~rnapeopl/.

1046-2023/01 $35.00

in regulation of satellite RNA replication; group I introns (4) and group II introns (7), which catalyze two disparate steps during self-splicing with distinct structural requirements; and the ribosomal RNAs, which presumably undergo large-scale conformational changes to translocate the messenger RNA/transfer RNA hybrid after correct decoding of an amino acid and transfer of the growing peptide chain onto the A-site tRNA (8). The question of how these RNA structural transitions occur is closely linked to the problem of how an RNA sequence can specify a three-dimensional fold in the first place (the so-called RNA folding problem) (9–12). These problems can exquisitely be attacked by the fluorescence techniques discussed here.

Fluorescence resonance energy transfer (FRET), also called Förster transfer after Theodor Förster who quantitatively described the phenomenon in the 1940s (13), originates from a nonradiative dipole–dipole interaction between a donor and an acceptor fluorophore. The strong dependence of the energy transfer rate k_T and hence the energy transfer efficiency E_T on the donor–acceptor distance R, with

$$k_T = \frac{1}{\tau_D}\left(\frac{R_0}{R}\right)^6 \quad [1]$$

and

$$E_T = \frac{R_0^6}{R^6 + R_0^6} \quad [2]$$

(τ_D, donor fluorescence lifetime in the absence of acceptor; R_0, Förster distance at which E_T is 50%; R_0 is dependent on the spectral overlap of the fluorophore pair used and typically has a value of 20–90 Å), enables the calculation of fluorophore distances in the range 10–100 Å from their energy transfer efficiency. When two fluorophores are covalently tethered to defined sites on a biomolecule, or on two molecules in a complex, the distance between these sites can be measured (for more information on the basics of FRET see (14)). The distance range accessible by FRET is ideal for many biological macromolecules and fills the gap between that of other techniques, such as NMR and electron microscopy.

Over the years, many excellent reviews have been written on FRET as a technique for structural analysis of biomolecules (15–28) (see also several articles in this issue). In the context of RNA, FRET had been used early on for analyzing ribosome function (reviewed in (29)). For example, in the course of translation, changes in distance between two tRNAs or a tRNA and a ribosomal protein in the assembled tRNA–ribosome complex were observed (30). Likewise, the topology of ribosome-bound messenger RNA with respect to the 3′ end of 16S ribosomal RNA was evaluated by labeling the 5′ or 3′ end of various mRNA fragments with one and the 3′ end of 16S rRNA with the other fluorophore of a FRET pair (31, 32). More recently, FRET has been applied to distance measurements in smaller and better defined RNA structures, such as RNA two-, three-, and four-way junctions (33–38), tRNA (39), and the hammerhead ribozyme (40, 41). In principle, the donor–acceptor distances obtained can be used as constraints in molecular modeling of the underlying RNA architecture in the absence of a high-resolution NMR or crystal structure (40, 42). However, the precision of the derived molecular models is sometimes limited (43) due to the uncertainty in the relative orientation of the two fluorophores and in their exact locations because of their finite sizes and considerable tether flexibility (19, 29).

A particular appeal of fluorescence techniques is that they yield a continuous and highly sensitive signal that can report on dynamic changes in real time. As a result, many high-throughput screening techniques rely on fluorescence assays (44). For example, cleavage by the hammerhead ribozyme and subsequent product dissociation can directly be followed as a breakdown of energy transfer between a donor and acceptor fluorophore on the substrate (45, 46) or on the substrate and ribozyme (47). These assays have potential applications in high-throughput screening for effectors of ribozyme activity (48).

Directly aimed at improving our understanding of RNA structural dynamics are recent advances in observing the tertiary structure transitions of the hairpin ribozyme by FRET (6, 36, 38, 49–51), which are reviewed here. I focus on how to adapt new RNA systems to the use of FRET-based techniques, with the hairpin ribozyme as the pioneering example (for recent, more comprehensive overviews over the use of FRET on RNA see (25, 27, 28)). Similar domain docking events as seen in the hairpin ribozyme can be expected to be at the heart of the folding and biological function of many RNAs, making the hairpin ribozyme a paradigm for our understanding of RNA structural dynamics (5, 6, 9, 35, 36, 52). The versatility of the fluorescence labeling and analysis techniques described here will most certainly guarantee their increasing popularity in the "RNA World."

DESCRIPTION OF METHOD

1. Getting Started: Designing the RNA System

Figure 1 summarizes a strategy to adapt a new RNA system to the use of FRET techniques that was tested on the hairpin ribozyme. First, one has to decide on the

RNA sequence to study. Often, it might be useful to start with a "wild-type" or previously characterized sequence, but it is advisable to check whether this sequence is predicted to fold homogeneously, e.g., using Michael Zuker's RNA folding software "mfold version 3.0" (http://bioinfo.math.rpi.edu/~mfold/rna/form1.cgi) (53). In the case of the hairpin ribozyme, for example, self-complementarity of the wild-type substrate was discovered and could be eliminated by careful redesign of the substrate and substrate-binding strands, under retention of all conserved base positions (54). This modification led to improved catalytic (55) and structural behavior (52).

Unlike proteins, most RNAs do not contain intrinsic fluorophores (25). Hence, the most efficient way to site-specifically introduce the two fluorophores necessary for FRET is by synthesizing the fluorophore-containing RNA strand(s). The fluorophore can be added either during or after synthesis; in the latter case, a functional group is introduced that allows for subsequent coupling to a reactive fluorophore derivative. Detailed descriptions of the many synthetic strategies possible are given elsewhere (25, 56). Briefly, solid-phase RNA synthesis in the $3' \rightarrow 5'$ direction based on phosphoramidite chemistry can be modified to introduce:

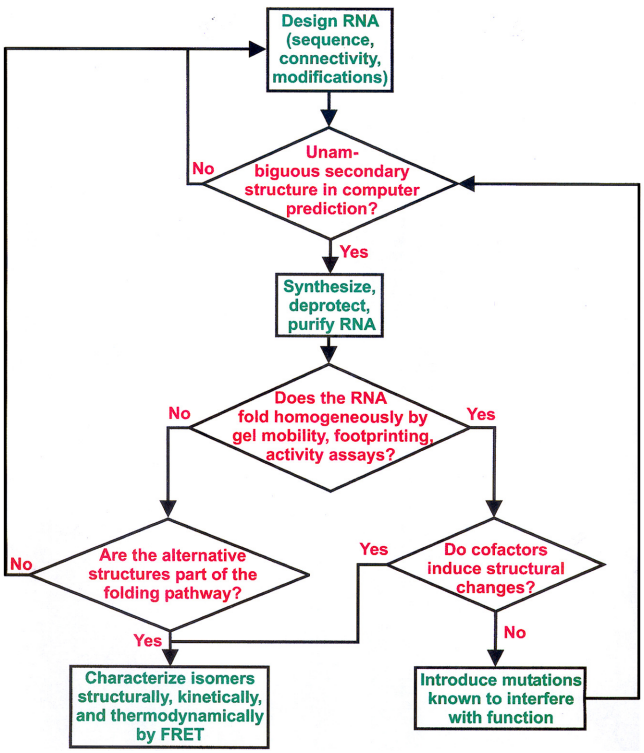

FIG. 1. Iterative procedure to adapt a new RNA system to the use of FRET for studying its structural dynamics.

(a) fluorophore derivatives that are resistant to RNA deprotection chemistry, such as fluorescein and cyanine phosphoramidites, on the 5′ end;

(b) fluorophores that are resistant to the coupling and deprotection chemistries, such as fluorescein and pyrene, on the 3′ end and internally, using column supports and nucleotide phosphoramidites, respectively, modified with linkers carrying the fluorophore;

(c) aliphatic amino or thiol linkers on the 5′ or 3′ end, or internally, that can postsynthetically be coupled under mild conditions with derivatives, such as amino-reactive succinimidyl esters and thiol-reactive maleimides, of chemically sensitive fluorophores, such as rhodamines.

New variations of these themes are continuously being developed, for example, the use of a site-specific phosphorothioate modification for internal labeling (57). Assembling the RNA on an automated DNA/RNA synthesizer (from, e.g., PE Applied Biosystems, Foster City, CA; *www.appliedbiosystems.com*), using β-cyanoethyl phosphoramidite supplied by companies such as Glen Research (Sterling, VA; *www.glenres.com*), ChemGenes (Ashland, MA; *www.chemgenes.com*), Clontech (Palo Alto, CA; *www.clontech.com*), Amersham Pharmacia Biotech (Piscataway, NJ; *www.apbiotech.com*), Cruachem (Glasgow, UK; *www.cruachem.com*), Dalton Chemical Laboratories Inc. (Toronto, ON; *www.dalton.com*), and PE Applied Biosystems is quite straightforward. More expensive, yet very convenient is the use of commercial suppliers of synthetic RNA, of which there are a few, e.g., Dharmacon (Boulder, CA; *www.dharmacon.com*), Xeragon (Zürich, Switzerland; *www.xeragon.ch*), Midland Certified Reagent Co. (Midland, TX; *www.mcrc.com*), Cruachem, the Keck Foundation's Biotechnology Resource Laboratory at the Yale University School of Medicine (*info.med.yale.edu/wmkeck/oligos.htm*). Many reactive fluorophore derivatives for postsynthetic labeling of RNA are available from Molecular Probes (Eugene, OR; *www.probes.com*) or Sigma–Aldrich (St. Louis, MO; *www.sigma-aldrich.com*), while succinimidyl esters of the cyanine dyes currently may be obtained only from Amersham Pharmacia Biotech.

At present, the length of a synthetic RNA is restricted to about 50 nt due to limited coupling efficiency per nucleotide cycle. One way to overcome this limitation is to change the RNA strand connectivity; in the case of the hairpin ribozyme, this led to the use of a two-partite ribozyme with fluorophores on the 5′ and 3′ ends of the 32-nt-long 5′ segment, which binds a 21-nt 3′ segment and a 14-nt substrate (Fig. 2a). Alternatively, longer RNAs bearing an internal FRET fluorophore pair can be constructed by, e.g., ligating a synthetic,

fluorophore-labeled strand with longer RNAs derived from natural sources or *in vitro* transcription, using T4 DNA ligase and a DNA splint (for review see (56, 58)).

The choice of fluorophores, labeling sites, and tether lengths depends on availability, compatibility with biological function, and the requirements of the experiments intended. Specific examples are given below for the hairpin ribozyme. In general, the following considerations should be taken into account:

a. Each donor–acceptor pair is characterized by a specific Förster distance R_0 (14, 18); according to Eq. [2] changes in FRET efficiency are at a maximum for distance changes around R_0; hence, choosing a fluorophore pair whose R_0 is close to the measured distance will increase the sensitivity toward distance changes.

b. For certain requirements, specific donor–acceptor pairs may be better suited than others; for example, high labeling yields can be obtained with fluorophores incorporated during synthesis (6); a small overlap of the donor and acceptor emission spectra simplifies their spectral separation if the contribution of just one fluorophore needs to be extracted for distance measurements (17, 36); while high photostability is a strong selection criterion for single-molecule FRET pairs (59).

c. If structural transitions are to be observed, the location of the fluorophores should be chosen so as to maximize the expected distance changes.

d. If information on the three-dimensional structure is available, this should be used to choose a labeling site expected to minimally interfere with biological function.

e. Often, the emission of an excited fluorophore is quenched by a proximal nucleobase through an outer-sphere electron transfer between the two species; according to Marcus theory (60), the rate of this quenching is governed by the frequency of diffusional encounters of and the activation barrier for redox chemistry between the excited fluorophore and the base (61); therefore, the choice of RNA sequence immediately adjacent to the fluorophore (and, to some extent, the fluorophore tether length (62)) has an influence on quenching; for example, both fluorescein (54) and tetramethylrhodamine (63), a popular FRET pair, are quenched by guanine; this nucleobase-specific quenching has been used to observe secondary structure formation (6, 54), yet it is better avoided to allow for absolute distance measurements by time-resolved FRET (25, 36).

f. A sufficient length of the fluorophore tethers is necessary to ensure their conformational flexibility, indicated by a low fluorescence anisotropy (14); flexibility

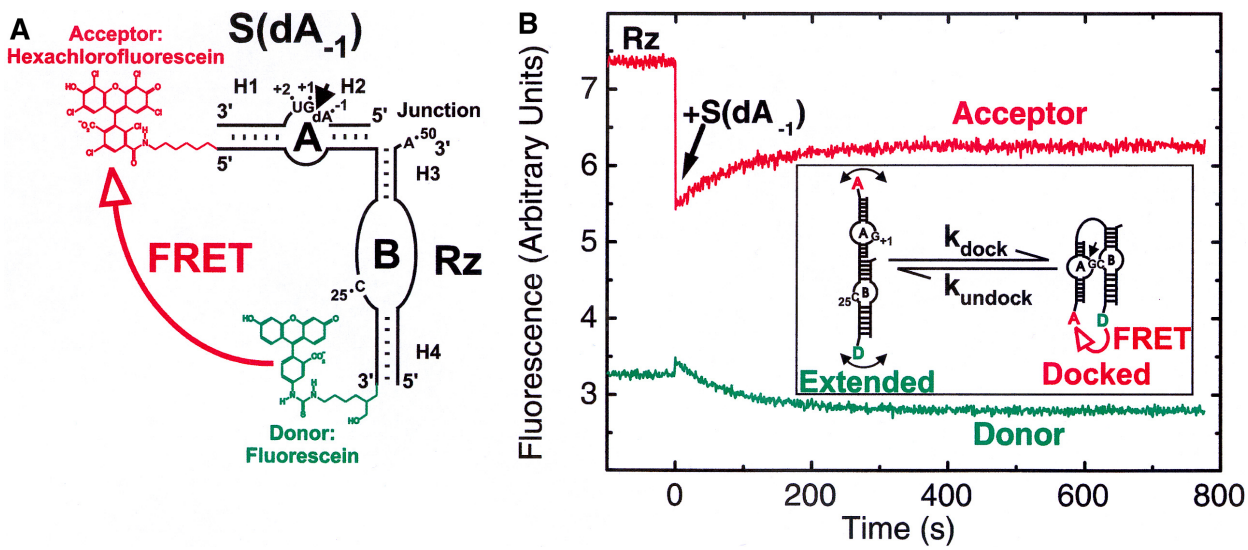

FIG. 2. Analysis of the docking kinetics of the hairpin ribozyme–substrate complex by FRET. (A) The doubly labeled ribozyme–substrate complex used for energy transfer measurements. The two-strand hairpin ribozyme (Rz) binds the noncleavable substrate analog S(dA$_{-1}$) to form domain A, comprising Watson–Crick base paired helices H1 and H2 and the symmetric internal loop A. This domain is joined through a flexible junction to domain B of the ribozyme containing helices H3 and H4 and an asymmetric internal loop B. A donor and acceptor pair is coupled to the 3′ and 5′ ends of the 5′ half of the two-strand ribozyme to enable distance-sensitive FRET (open arrow). The short arrow indicates the potential cleavage site. Numbered nucleotides are referred to in the text. (B) Fluorescence signals over time as a result of domain docking in the ribozyme–substrate complex. The doubly labeled ribozyme displays a strong signal for the acceptor fluorophore and a weaker one for the donor. On manual addition of a tenfold excess of noncleavable substrate analog, significant quenching of the acceptor fluorescence is observed due to rapid ribozyme–substrate complex formation. Subsequently, the acceptor signal increases, while the donor signal decreases at the same rate, indicating reversible transition from an extended to a docked conformation (inset).

becomes important for absolute distance measurements between donor and acceptor from Eq. [2], since the orientation factor κ^2 has to be known to be able to calculate the Förster distance R_0 from

$$R_0^6 = 8.79 \times 10^{-28} \Phi_D \kappa^2 n^{-4} J(\lambda) \quad (\text{in } \text{Å}^6) \qquad [3]$$

(Φ_D, donor fluorescence quantum yield in the absence of acceptor; n, refractive index of medium; $J(\lambda)$, spectral overlap integral of donor emission and acceptor absorption); κ^2 has a defined value of 2/3 if the fluorophore transition dipole moments have a random relative orientation during energy transfer (14); alternatively, κ^2, which can range from 0 to 4, would be known for a completely fixed relative fluorophore orientation; however, this is difficult to achieve in a solution-based system (64).

Once the RNA sequence, strand connectivity, and modifications are chosen, the RNA is synthesized, and then needs to be deprotected and purified (Fig. 1). Again, more detailed accounts have been given elsewhere (25). In short, a fairly mild deprotection procedure that appears to be compatible with most fluorophores added during synthesis is the following:

(a) incubation for 4 h at 65°C in 1 ml of a 3:1 mixture of concentrated aqueous ammonia and ethanol (to remove the exocyclic amine protection groups),
(b) drying in a lyophilizer,
(c) 20 h tumbling at room temperature with 800 μl triethylamine trihydrofluoride (to remove the 2′-OH silyl protection groups), and
(d) precipitation with 1-butanol, washing with ethanol, and careful drying to remove traces of 1-butanol that interfere with gel electrophoresis.

Recent advances in protection chemistry have considerably improved the yield and ease of deprotection (65), especially since this 2′-orthoester-protected RNA is commercially available (Dharmacon). In any case, full-length RNA is obtained by purification on a denaturing (8 M urea) 20% polyacrylamide gel. Subsequent C_8 reversed-phase HPLC in 100 mM triethylammonium acetate, with linear elution gradients of 0–40 and 0–60% acetonitrile (50 min, 1 ml/min) for unlabeled and labeled strands, respectively, removes not fully deprotected material and other contaminants. Under these conditions, fluorophore-labeled RNA is considerably retarded relative to unlabeled RNA. If desired, fluorophores may be coupled to aliphatic amino and thiol groups at this stage. Subsequently, the labeled RNA is recovered by ethanol precipitation and extensive washing with 80% ethanol, and is repurified by C_8 reversed-phase HPLC. To obtain an accurate concentration for labeled RNA, the additional absorbance of the fluorophores at 260 nm should be taken into account with, e.g., $A_{260}/A_{492} = 0.3$ for fluorescein, $A_{260}/A_{535} = 0.3$ for hexachlorofluorescein, and $A_{260}/A_{554} = 0.49$ for tetramethylrhodamine (25).

At this stage, it is important to check the synthetic RNA for homogeneous folding and proficient biological function (Fig. 1). An easy way to test for homogenous folding is to run a nondenaturing gel mobility assay; for simplicity, electrophoresis can be performed with nonfluorescent control RNA. In the case of the hairpin ribozyme, a 10% polyacrylamide gel in 40 mM Tris–HOAc, pH 7.5, 25 mM $Mg(OAc)_2$, run at 10 V/cm and 4°C, proved suitable to observe the homogeneity of a ribozyme–substrate complex formed from trace amounts of 5′-^{32}P-labeled, noncleavable substrate analog and an excess of ribozyme in a variety of buffers (66). Oftentimes, such gels can serve a second, even more important purpose: Depending on their rate of interconversion, native gels may reveal alternative tertiary structures that are part of the RNA folding pathway (67, 68). These are precisely the structures that ought to be further characterized by FRET (Fig. 1). Alternatively, structural changes as observable by altered gel mobility may be induced by the addition of cofactors (67), or the introduction of mutations known to interfere with activity (69). In the case of the hairpin ribozyme, biphasic reaction kinetics revealed the presence of two distinct conformers, an inactive extended and an active docked ribozyme–substrate complex (55, 70). Mutation of an essential guanosine immediately 3′ of the substrate cleavage site was found by FRET to interfere with folding from the extended to the docked conformation (6) (see also Section 2). Other structure-probing techniques such as hydroxyl radical (52) and terbium(III)-mediated footprinting (51) as well as photoaffinity crosslinking (71) were used to further characterize these alternate conformers. It is this combination of biochemical and biophysical techniques, performed in an iterative fashion (Fig. 1), that has provided us with a detailed picture of the interplay of folding and function in the hairpin ribozyme.

Under the assumption that they will be applicable to many other RNA systems designed based on the rules above, the FRET techniques developed for the hairpin ribozyme will be described in the following. First, a steady-state FRET assay to observe relative structural changes is discussed; it avoids many complications associated with measuring absolute distances while exploiting the capability of FRET to study processes in real time.

2. Laying the Ground: Steady-State FRET to Observe RNA Conformational Changes

A minimal reaction pathway of a ribozyme that cleaves an external substrate is composed of three reversible steps: substrate binding, cleavage, and product dissociation (55, 72). Based on previous linker insertion studies of the junction between the two independently folding domains A and B of the hairpin ribozyme–substrate complex (5), we suspected that a conformational change, docking of the two domains, occurred after binding and before the chemical step of the reaction. To observe this structural transition by FRET, we used a two-strand version of the hairpin ribozyme and labeled its 5′ segment with a 5′-hexachlorofluorescein acceptor and a 3′-fluorescein donor fluorophore (Fig. 2a) (we found later that other fluorophore pairs work just as well). This design ensures the presence of exactly equimolar amounts of both fluorophores. A 10-fold molar excess of the 3′-ribozyme segment was annealed with the 5′ segment by heating to 70°C for 2 min, followed by cooling down to room temperature over 5 min, to saturate the fluorescently labeled strand (typically used at 20–50 nM for a good signal-to-noise ratio).

Steady-state fluorescence spectra and intensities were recorded on an Aminco–Bowman Series II spectrofluorometer from Spectronic Unicam (Rochester, NY; *www.spectronic.com*) in a cuvette with 3-mm excitation and emission path lengths (150-μl total volume). This instrument allows for the parallel detection of both fluorophores during a time course, by continually shifting the emission monochromator back and forth. Water to set up buffer solutions was degassed and argon-saturated to minimize photobleaching of the fluorophores over extended excitation times. In addition, buffers were typically supplemented with 25 mM dithiothreitol (DTT) as radical quencher and singlet oxygen scavenger (73). Sample temperature was regulated by a circulating water bath, taking the temperature difference between bath and cuvette content into account.

Both substrate (here and in the following, unless otherwise stated, we used a noncleavable substrate analog with a deoxy modification at the cleavage site, S(dA$_{-1}$), that shows undisturbed structure formation) and assembled ribozyme were separately preincubated for 15 min in buffer (typically 50 mM Tris–HCl, pH 7.5, 12 mM $MgCl_2$, 25 mM DTT), at the reaction temperature (typically 25°C). Fluorescence data acquisition was started, and hairpin ribozyme–substrate complex was formed by manually mixing 145 μl ribozyme solution in the fluorometer cuvette with 5 μl substrate stock solution (supplying a saturating 10-fold substrate excess). Alternatively, structural transitions can be induced by the addition of Mg^{2+}, or a stopped-flow reactor can be used to detect fast conformational changes that require rapid mixing.

In the case of the fluorescein/hexachlorofluorescein-labeled hairpin ribozyme, fluorescence emission values (typically one datum per second) for both donor (at 515 nm, F_{515}) and acceptor fluorophore (at 560 nm, F_{560}) were recorded using the fluorometer software package. First, on substrate addition, a strong acceptor quench and slight donor dequench were observed (Fig. 2b). At the same time, an increasing fluorescence anisotropy of the acceptor revealed the decreasing fluorophore mobility on substrate binding (6). Under the conditions used, substrate binding is fast and occurs within the manual mixing time (54). Because the fluorescence decrease was observed only with cognate substrate, we conclude that the rapid acceptor quench is mostly due to quenching of hexachlorofluorescein in the ribozyme–substrate complex, presumably by a base-specific electron transfer mechanism involving the 3′-terminal uracils of the substrate (54).

Subsequently, the donor fluorescence decreased over several minutes, while the acceptor fluorescence increased at the same rate. This observation strongly suggests that the underlying molecular process involves increasing FRET between the two fluorophores, as expected for their approach on domain docking in the ribozyme–substrate complex (Fig. 2b). From the temporal change in the ratio $Q = F_{560}/F_{515}$, a relative measure of FRET efficiency, the rate constant of the transition between extended and docked complex could be extracted and its dependence on RNA and buffer modifications studied (6). It is important to note that, for a reversible docking step, the observed docking rate constant $k_{dock,obs}$ of (0.64 ± 0.04) min^{-1} under standard conditions is a combination of at least the elementary docking and undocking rate constants:

$$k_{dock,obs} = k_{dock} + k_{undock}. \quad [4]$$

$k_{dock,obs}$ can be further dissected only by an independent measurement of the docking equilibrium constant (possible by time-resolved FRET, see Section 3) or the undocking rate constant (possible in single-molecule experiments, see Section 4). A measured fraction of 65% docked ribozyme–substrate complex under standard conditions (see Section 3) leads to estimates for k_{dock} and k_{undock} of 0.53 and 0.32 min^{-1}, respectively. That makes docking into an active ribozyme–substrate complex about 3.5 times faster than cleavage and, therefore, at the most partially rate-limiting (6).

Strikingly, most modifications to the RNA or reaction conditions that inhibit catalysis do so by interfering with docking. For example, substitution of the guanosine immediately 3′ of the cleavage site (G_{+1}) with A,

C, or U results in profound inhibition of the reaction (74). Use of the $G_{+1}A$ variant in the FRET assay showed that the modified substrate binds to the substrate-binding strand, as indicated by quenching of the ribozyme's 5′-hexachlorofluorescein. However, no subsequent increase in FRET was observed, in contrast to the complex with the wild-type S(dA$_{-1}$) substrate (Fig. 3a). Therefore, we could conclude that the mechanism of inhibition by the $G_{+1}A$ substitution involves blocking of the essential domain docking step. When a second mutation, $C_{25}U$, was introduced into domain B, catalytic activity was largely restored, despite the fact that still no docking was observed. In general, all Watson–Crick-type combinations between the substrate +1 and ribozyme 25 positions showed a similar behavior, strongly suggesting the existence of a transient interaction between these positions (50).

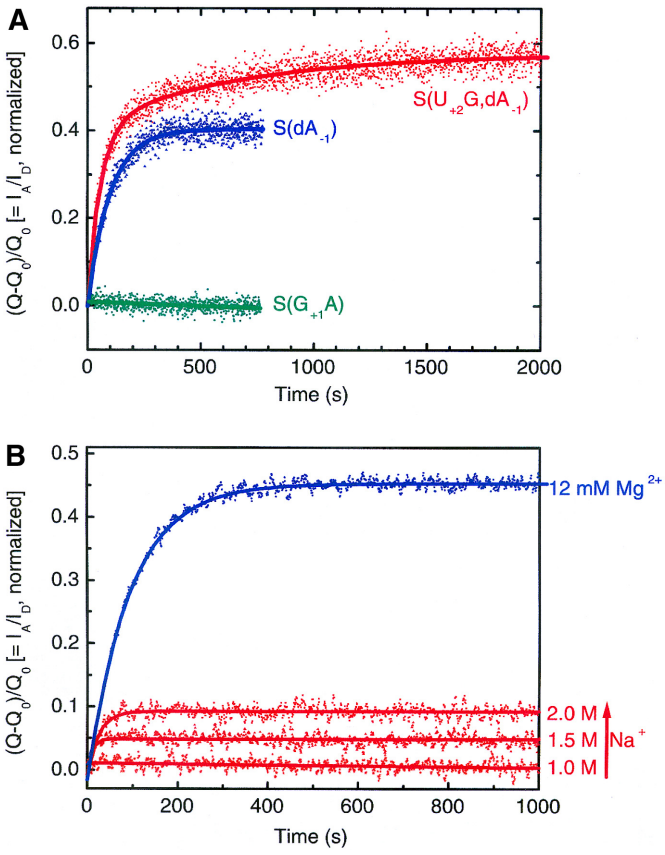

FIG. 3. Domain docking under a variety of conditions. (A) Docking of complexes between hairpin ribozyme and substrate variants. The noncleavable wild-type substrate analog S(dA$_{-1}$) leads to a single-exponential increase in the normalized ratio of acceptor (I_A) over donor (I_D) fluorescence, a measure of the relative FRET efficiency. In the presence of a $G_{+1}A$ mutation, no signal increase is observed, while a noncleavable substrate analog with a $U_{+2}G$ mutation results in a double-exponential increase (solid lines, fits). (B) Docking of wild-type ribozyme–substrate complex in the presence of high monovalent cation concentrations. At up to 1 M Na^+, no significant change in the relative FRET efficiency is observed, while 1.5 and 2 M Na^+ lead to detectable signal increases, indicative of significant docking. These FRET increases are less pronounced than in the presence of the standard 12 mM Mg^{2+}, yet they provide direct evidence for interaction of the domains of the ribozyme–substrate complex in the presence of molar concentrations of monovalent cations.

For a substrate variant with a $U_{+2}G$ mutation, cleavage activity is decreased fourfold (74), but domain docking remains efficient. However, the FRET signal increase clearly displays a second, slower phase, a unique feature among all tested modifications of sequence or conditions (Fig. 3a). This second phase leads to a higher overall amplitude of the FRET increase which can be correlated with a higher abundance of docked complex. This observation invokes a mechanism of functional interference by a $U_{+2}G$ mutation, in which the ribozyme–substrate complex becomes trapped in a native-like docked fold, proceeding only slowly to the transition state (75).

We also used the steady-state FRET assay to compare docking of ribozyme–substrate complex domains A and B under a variety of ionic conditions. As expected, divalent metal ions that promote catalytic activity, such as Mg^{2+}, Ca^{2+}, and Sr^{2+}, lead to efficient docking (6). Significantly, high (> 1 M) concentrations of monovalent cations, such as Na^+, also promote efficient cleavage and docking (49) (Fig. 3b). These results support earlier evidence that metal ions are not obligatory chemical participants in the reaction catalyzed by the hairpin ribozyme (5). They rather appear to assist the RNA in folding into an active docked conformation by neutralizing its negative backbone charges. With all likelihood, the RNA fold itself then contributes all functional groups necessary for catalysis. Interestingly, the lanthanide ion terbium(III) interferes with catalysis by competing for an essential cation binding site in domain B, yet it does not block domain docking as observed by steady-state FRET (51).

These results demonstrate the versatility of a steady-state FRET assay to directly observe the kinetics of an RNA folding event in solution under a variety of conditions. Analyses using time-resolved FRET can strongly complement these data by supplying information on the relative stability and the structural characteristics of the conformers involved.

3. Time-Resolved FRET Reveals RNA Conformers in Equilibrium

There are a number of techniques for calculating the energy transfer efficiency E_T from the spectroscopic properties of a donor–acceptor pair (17). One can measure:

(a) the enhanced fluorescence of the acceptor;
(b) the decreased fluorescence quantum yield of the donor;
(c) the change in fluorescence anisotropy of the donor and acceptor; or
(d) the decrease in donor fluorescence lifetime.

Once E_T is determined and R_0 is obtained from Eq. [3], Eq. [2] can be used to calculate the donor–acceptor distance to gain insight into the architecture of the RNA to which the fluorophores are coupled. However, most methods will yield a single E_T value from which a single donor–acceptor distance is derived. That contrasts with the fundamental structural dynamics any biomolecule displays in solution. For an RNA molecule, in particular, large-scale conformational dynamics have to be taken into account as part of its biological function. In addition, the fluorophore tethers contribute to the range of molecular motions of donor and acceptor.

Haas, Steinberg, and co-workers have pioneered the use of time-resolved FRET (trFRET) to reveal the conformational dynamics in polypeptides (76). The idea is simple: On the time scale of a typical donor fluorophore lifetime in the excited state (nanoseconds), any molecular motion is slow and the donor–acceptor distance appears fixed. Therefore, each individual donor–acceptor distance will be characterized by a unique donor fluorescence lifetime. A flexible molecule population will display a range of donor–acceptor distances that reveals itself in a mixture of donor lifetimes. If the donor fluorescence decay is determined with high enough precision, the underlying range of donor–acceptor distances can be resolved (14).

trFRET has been successfully used to extract distance distributions from proteins and oligosaccharides (for review, see (14)). Millar and co-workers have applied the technique to DNA, especially junction structures (reviewed in (23)), showing that a four-way, so-called Holliday junction exists as an equilibrium mixture of two conformational isomers (77). This analogy prompted us to investigate the hairpin ribozyme by trFRET.

To this end, a 5′-fluorescein donor and a 3′-tetramethylrhodamine acceptor were attached to the construct used for the previous steady-state FRET study (36). The attachment site of the donor next to A:U base pairs ensured the absence of quenching effects by guanine, simplifying lifetime data analysis; the choice of a rhodamine allowed for clean optical separation of the acceptor emission. RNA complexes were prepared in standard buffer (50 mM Tris–HCl, pH 7.5, 12 mM $MgCl_2$) with the fluorophore-labeled strand in 1 μM concentration and all other strands in a saturating 3-fold excess (10-fold in the case of the cleavage product analogs). The mixture was heat-denatured for 2 min at 70°C, then allowed to cool to room temperature over 5 min. The sample (150 μl) was incubated in a quartz cuvette at measurement temperature (standard: 17.8°C) for at least 15 min, prior to collecting time-resolved emission profiles of the fluorescein donor using time-correlated single-photon counting (14). Excitation was at 514.5 nm with 90-ps-duration pulses, picked down to 1.87 MHz, from a mode-locked argon-ion laser (Coherent Innova 100-12); isotropic emission detection to >40,000 peak counts was performed under magic angle polarizer conditions at 530 nm (single-grating monochromator with 16-nm slit width plus 530-nm-cutoff filter). Decays were typically collected in 2048 channels with a sampling time of 18.0 ps/channel, using a microchannel plate photomultiplier (Hamamatsu R2809U-01) feeding into a time-correlated single-photon counting system with multichannel analyzer (Ortec). An instrument response function was measured as the scattering signal from a dilute solution of nondairy coffee creamer. This function was used to deconvolute the fluorescence decay data (36).

It is important to note that the conditions used to obtain these high-precision decay data require a significant acquisition time of tens of minutes. Hence, only samples in thermodynamic equilibrium can be studied. "Time-resolved" FRET therefore refers to the fact that fluorescence decay data are measured, while the FRET efficiency needs to remain constant over time to obtain meaningful data.

To derive distance information, two time-resolved fluorescence decays were collected: one for the sample with acceptor in place, one under identical conditions but employing a donor-only RNA complex. The time-resolved decay of fluorescein emission in the donor-only complex was used to extract the two or three intrinsic donor lifetimes τ_i with their fractional contributions α_i by a sum-of-exponentials fit. The data from the doubly labeled complex $I_{DA}(t)$ were then fitted with a model for distance distributions,

$$I_{DA}(t) = \sum_k f_k \int P_k(R) \sum_i \alpha_i \exp\left[-\frac{t}{\tau_i}\left(1 + \left(\frac{R_0}{R}\right)^6\right)\right] dR, \quad [5]$$

where the first sum refers to the number of distributions, either one or two, each with fractional population f_k and distance distribution $P_k(R)$. Distance distributions were modeled as weighted gaussian,

$$P(R) = 4\pi R^2 c \exp[-a(R - b)^2], \quad [6]$$

where a and b are parameters that describe the shape of the distribution and c is a normalization constant.

Equation [5] was used to fit experimental data by nonlinear least-squares regression, with a, b, and f_k for each distribution as adjustable parameters. The τ_i and α_i values from the donor-only decay were used under the assumption that each intrinsic donor lifetime is influenced independently by the presence of the acceptor in distance R and is split into a lifetime distribution by the distribution in R.

Two distance distributions were used for analysis when a single distribution failed to give a good fit, as judged by the reduced χ^2 value and by inspection of residuals. In all such cases the inclusion of a second distribution resulted in dramatic improvement of the fit. The Förster distance R_0 was evaluated for the donor–acceptor pair ($R_0 = 55$ Å) according to Eq. [3] and assuming a value of 2/3 for the orientation factor. The latter assumption was supported by time-resolved fluorescence anisotropy decay experiments that revealed large-amplitude rotational motions of both fluorescein and tetramethylrhodamine (36).

Using trFRET, we were able to neatly resolve the equilibrium distribution between the two hairpin ribozyme conformational isomers in solution (Fig. 4). Sixty-five percent of the wild-type population reside in the active docked conformation with a mean donor-acceptor distance of 34 Å (FWHM, 18 Å), while 35% of the population adopt the inactive extended conformation with a distance of 78 Å (FWHM, 18 Å). As a control and consistent with the previous steady-state FRET experiments (see Section 2), a $G_{+1}A$ mutant ribozyme–substrate complex revealed a pattern of donor lifetimes indicative of a single, extended conformation.

It is important to note that other methods that yield RNA structural information often fail to do so on conformer mixtures. By contrast, trFRET extracts distances between donor–acceptor labeling sites on the two hairpin ribozyme conformers, useful for molecular modeling purposes, and also quantifies their relative abundance in equilibrium (36).

Application of trFRET to resolve and quantify the distribution between docked and extended conformers defines the equilibrium constant for docking K_{dock}:

$$K_{dock} = \frac{\text{docked fraction}}{\text{undocked fraction}} = \frac{k_{dock}}{k_{undock}}. \qquad [7]$$

Together with Eq. [4] and the kinetic data presented in Section 2, the elementary docking and undocking rate constants k_{dock} and k_{undock}, respectively, are accessible. In addition, the associated free energy difference $\Delta G_{dock} = -RT \ln(K_{dock})$ between the two structurally defined minima in the folding free energy landscape of the hairpin ribozyme can be calculated (36). We found that mutations, the nature of the helical junction between domains A and B, and changes in metal ion concentration can shift the equilibrium distribution between docked and extended conformers from an undetectable (<2%) to a strongly prevalent (95%) docked fraction. Accordingly, ΔG_{dock} ranges between +2.3 and −1.7 kcal/mol, and can be measured by trFRET with high precision.

Connecting the wild-type substrate to the ribozyme to form a bulged two-way junction slightly stabilizes the docked conformer by 0.28 kcal/mol, consistent with

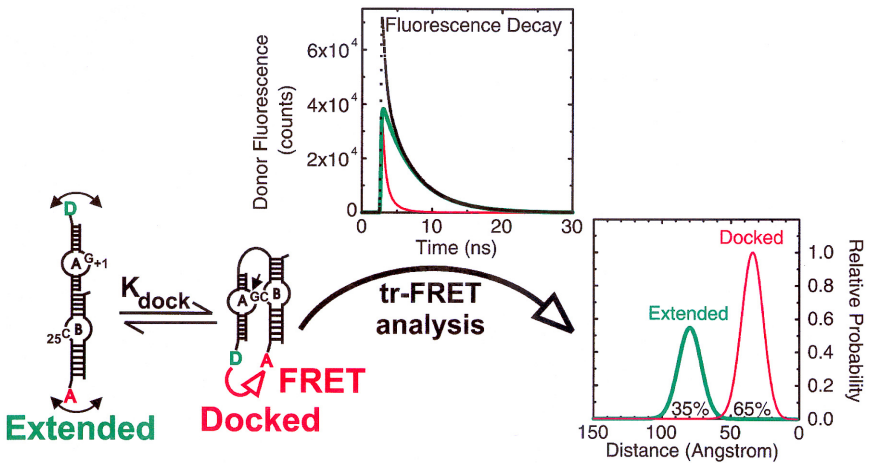

FIG. 4. Revealing the equilibrium between the extended and docked conformers of the hairpin ribozyme by trFRET. If the complex can fold from the initial extended structure into the docked conformer (in the presence of the wild-type G_{+1}:C_{25} interaction) the donor decay data (dots) can only be fitted assuming lifetime contributions from two gaussian donor–acceptor distance distributions, revealing the presence of both extended and docked conformers; the deconvoluted contributions to the donor decay from the extended and docked conformers are represented by thick and thin lines, respectively. The relative abundance of these isomers is obtained directly from the analysis and is reflected in the relative peak areas of the corresponding distance distributions.

previous observations that bulges impose bends into RNA helical junctions (36). Adding a third and forth helix to the junction, forming three- and four-way junction constructs, respectively, yielded some unexpected findings: The four-way junction strongly favors formation of the docked complex under standard conditions, leading to an equilibrium in which 95% of the molecules are docked. In contrast, a three-way junction was found to lead to only 39% docked complex (36).

Under physiological conditions (ca. 1 mM Mg^{2+}), the relative enhancement of hairpin ribozyme folding by the four-way junction is still more dramatic. Here, the two-way junction yields only 8% docked complex, while the four-way junction is characterized by more than 90% docked conformation. Similarly for the temperature dependence, the four-way junction favors docking at significantly higher temperatures than does the two-way junction (36). In an elegant follow-up study it was shown that the higher tertiary structure stability observed for the four-way junction is the result of a lower entropic cost of the docking process (38). It comes as little surprise, therefore, that nature has chosen a four-way junction as the architectural framework of the hairpin ribozyme in the satellite RNA of the tobacco ringspot virus (5).

Finally, a religation of previously cleaved RNA is part of satellite RNA replication *in vivo*, and requires assembly of a ternary complex for *trans* reactions *in vitro*. In the presence of saturating concentrations of cleavage product analogs, the global structures of the extended and docked complexes and their equilibrium position were found to be virtually identical to those observed with the cleavage substrate. This observation indicates that the docked structure does not change significantly on cleavage and that the energy differences between docked and extended complexes are the same for cleaved and intact substrates (36).

In summary, these results prove trFRET to be an elegant tool to study the free energy landscape associated with folding of a catalytic RNA from a defined intermediate to a native conformer. The flexibility in the molecule population is revealed and the mean intramolecular distances that are derived may serve as constraints in molecular modeling of the underlying RNA architecture. Our next level of understanding will come from studying individual molecules of the RNA population by single-molecule FRET (see also article in this issue by Ha).

4. Prospects Beyond Ensemble Measurements: Steady-State FRET on Single RNA Molecules

Steve Chu and co-workers have recently developed methods to observe conformational dynamics of individual RNA molecules by FRET. A study of the hairpin ribozyme is currently underway (X. Zhuang, H. Kim, M. Pereira, N. G. Walter, and S. Chu, in preparation). In light of the recent review article by Weiss on single-molecule fluorescence spectroscopy (78) and a similar one by Ha in this issue of *Methods*, I confine the following discussion to the general relevance of this technique for catalytic RNA.

The steady-state and time-resolved FRET studies reviewed so far have revealed essential folding pathways of catalytic RNA. They directly tie in with classic studies of enzyme kinetics and are well within the realm of the experimental capabilities of many laboratories. By observing a molecule population in bulk they invoke an image of conformational rearrangements as a well-ordered set of events with ensemble-averaged characteristics. However, recent single-molecule studies of polymers have revealed the stochastic nature of folding events; identical molecules follow different pathways from one state to the next (79).

Single-molecule fluorescence experiments are experimentally challenging, yet they measure a number of qualities that are crucial for catalytic RNA folding. In principle, there are two avenues to such experiments:

(a) analysis of the laser-induced fluorescence bursts from molecules diffusing through the focal point of a confocal microscope (80–82) and

(b) fluorescence imaging of immobilized molecules using either scanning confocal microscopy with detection by avalanche photodiodes (37) or total internal reflection microscopy with detection by a CCD camera (59).

The latter study has focused on the folding and function of the *Tetrahymena* ribozyme that, despite being much larger, shares many general features with the hairpin ribozyme. As it turns out, RNA is quite amenable to single-molecule techniques since it does not suffer as much as proteins from nonspecific, denaturing adsorption to surfaces.

In their *Tetrahymena* ribozyme study, Chu, Herschlag, and co-workers labeled the RNA in two strategic positions with the highly photostable donor–acceptor pair Cy3 and Cy5 (59). Neither these modifications nor surface immobilization altered the catalytic activity of the RNA. On docking of the substrate binding duplex P1 into the ribozyme core (83), a substantial increase in the FRET efficiency was observed. Time traces of individual molecules revealed the dynamic nature of the equilibrium between the docked and undocked states, as the RNA continuously flips back and forth between these two conformations. The ensemble

docking and undocking rate constants were recovered as averages of the individual dwell times in the undocked and docked states, respectively. When a 2′-OH group of the substrate that is known to make a tertiary contact with the ribozyme core was masked with a methyl group, the docking equilibrium was shifted toward the undocked state; this manifested itself as a drastically decreased dwell time in the docked state, suggesting that the tertiary contact involving this 2′-OH group forms subsequent to the docking transition state (59).

These results establish single-molecule FRET as a powerful tool to examine folding pathways of catalytic RNA. In combination with ensemble measurements, very detailed kinetic and thermodynamic descriptions of the large-scale structural transitions that are essential for the function of many RNAs are within our reach.

CONCLUDING REMARKS

Recent advances have begun to exploit fluorescence resonance energy transfer as a tool to observe the dynamics of conformational changes in catalytic RNA. The very nature of RNA makes it an ideal target for these techniques, which were previously developed for proteins and subsequently transferred to DNA. Further developments in RNA synthesis and labeling, fluorescence spectroscopic equipment (including that for single-molecule experiments), flow cytometry, high-throughput screening, and chip-based complementary strand hybridization will help spread the use of the principles described here. The more RNA systems we study this way, the better we will understand the physicochemical properties of this fascinating, ubiquitous biopolymer.

ACKNOWLEDGMENTS

I thank John M. Burke and everyone in his laboratory, especially Erika Albinson, Raj Banerjee, Kirk Brown, Phil Chan, Jose Esteban, Mike Fay, Ken Hampel, Joyce Heckman, David Pecchia, Robert Pinard, Attila Seyhan, and Ning Yang, for their numerous contributions to the work described here, in the form of data and an enjoyable environment. I am also very grateful to David Millar for his collaboration on time-resolved FRET and to Steve Chu and Xiaowei Zhuang for introducing me to single-molecule FRET. The work described herein was supported by postdoctoral fellowships from the Alexander von Humboldt Foundation and the Max Planck Society as well as generous startup funds from the University of Michigan to N.G.W. and NIH grants to John M. Burke and N.G.W.

REFERENCES

1. Caprara, M. G., and Nilsen, T. W. (2000) *Nat. Struct. Biol.* 7, 831–833.
2. Gesteland, R. F., Cech, T. R., and Atkins, J. F. E. (1999) The RNA World, Cold Spring Harbor Laboratory Press, Cold Spring Harbor, NY.
3. Lilley, D. M. (1999) *Curr. Opin. Struct. Biol.* 9, 330–338.
4. Doherty, E. A., and Doudna, J. A. (2000) *Annu. Rev. Biochem.* 69, 597–615.
5. Walter, N. G., and Burke, J. M. (1998) *Curr. Opin. Chem. Biol.* 2, 24–30.
6. Walter, N. G., Hampel, K. J., Brown, K. M., and Burke, J. M. (1998) *EMBO J.* 17, 2378–2391.
7. Qin, P. Z., and Pyle, A. M. (1998) *Curr. Opin. Struct. Biol.* 8, 301–308.
8. Puglisi, J. D., Blanchard, S. C., and Green, R. (2000) *Nat. Struct. Biol.* 7, 855–861.
9. Treiber, D. K., and Williamson, J. R. (1999) *Curr. Opin. Struct. Biol.* 9, 339–345.
10. Tinoco, I., Jr., and Bustamante, C. (1999) *J. Mol. Biol.* 293, 271–281.
11. Woodson, S. A. (2000) *Cell. Mol. Life Sci.* 57, 796–808.
12. Westhof, E., and Fritsch, V. (2000) *Structure Fold Des.* 8, R55–R65.
13. Förster, T. (1948) *Ann. Phys. (Leipzig)* 2, 55–75.
14. Lakowicz, J. R. (1999) Principles of Fluorescence Spectroscopy, 2nd ed., Kluwer Academic, Norwell, MA.
15. Stryer, L., and Haugland, R. P. (1967) *Proc. Natl. Acad. Sci. USA* 58, 719–726.
16. Stryer, L. (1978) *Annu. Rev. Biochem.* 47, 819–846.
17. Clegg, R. M. (1992) *Methods Enzymol.* 211, 353–388.
18. Wu, P., and Brand, L. (1994) *Anal. Biochem.* 218, 1–13.
19. dos Remedios, C. G., and Moens, P. D. (1995) *J. Struct. Biol.* 115, 175–185.
20. Clegg, R. M. (1995) *Curr. Opin. Biotechnol.* 6, 103–110.
21. Selvin, P. R. (1995) *Methods Enzymol.* 246, 300–334.
22. McCarty, R. E. (1997) *Methods Enzymol.* 278, 528–538.
23. Yang, M., and Millar, D. P. (1997) *Methods Enzymol.* 278, 417–444.
24. Lankiewicz, L., Malicka, J., and Wiczk, W. (1997) *Acta Biochim. Pol.* 44, 477–489.
25. Walter, N. G., and Burke, J. M. (2000) *Methods Enzymol.* 317, 409–440.
26. Selvin, P. R. (2000) *Nat. Struct. Biol.* 7, 730–734.
27. Klostermeier, D., and Millar, D. P. (2000) *Methods*, in press.
28. Lilley, D. M., and Wilson, T. J. (2000) *Curr. Opin. Chem. Biol.* 4, 507–517.
29. Hardesty, B., Odom, O. W., and Picking, W. (1992) *Biochimie* 74, 391–401.
30. Odom, O. W., Picking, W. D., and Hardesty, B. (1990) *Biochemistry* 29, 10734–10744.
31. Bakin, A. V., Borisova, O. F., Shatsky, I. N., and Bogdanov, A. A. (1991) *J. Mol. Biol.* 221, 441–453.
32. Czworkowski, J., Odom, O. W., and Hardesty, B. (1991) *Biochemistry* 30, 4821–4830.
33. Gohlke, C., Murchie, A. I., Lilley, D. M., and Clegg, R. M. (1994) *Proc. Natl. Acad. Sci. USA* 91, 11660–11664.
34. Walter, F., Murchie, A. I., Duckett, D. R., and Lilley, D. M. (1998) *RNA* 4, 719–728.

35. Murchie, A. I., Thomson, J. B., Walter, F., and Lilley, D. M. (1998) *Mol. Cell* 1, 873–881.
36. Walter, N. G., Burke, J. M., and Millar, D. P. (1999) *Nat. Struct. Biol.* 6, 544–549.
37. Ha, T., Zhuang, X., Kim, H. D., Orr, J. W., Williamson, J. R., and Chu, S. (1999) *Proc. Natl. Acad. Sci. USA* 96, 9077–9082.
38. Klostermeier, D., and Millar, D. P. (2000) *Biochemistry* 39, 12970–12978.
39. Chan, B., Weidemaier, K., Yip, W. T., Barbara, P. F., and Musier-Forsyth, K. (1999) *Proc. Natl. Acad. Sci. USA* 96, 459–464.
40. Tuschl, T., Gohlke, C., Jovin, T. M., Westhof, E., and Eckstein, F. (1994) *Science* 266, 785–789.
41. Bassi, G. S., Mollegaard, N. E., Murchie, A. I., and Lilley, D. M. (1999) *Biochemistry* 38, 3345–3354.
42. Malhotra, A., Tan, R. K., and Harvey, S. C. (1994) *Biophys. J.* 66, 1777–1795.
43. Sigurdsson, S. T., Tuschl, T., and Eckstein, F. (1995) *RNA* 1, 575–583.
44. Sundberg, S. A. (2000) *Curr. Opin. Biotechnol.* 11, 47–53.
45. Singh, K. K., Parwaresch, R., and Krupp, G. (1999) *RNA* 5, 1348–1356.
46. Jenne, A., Gmelin, W., Raffler, N., and Famulok, M. (1999) *J. Am. Chem. Soc.* 38, 1300–1303.
47. Perkins, T. A., Wolf, D. E., and Goodchild, J. (1996) *Biochemistry* 35, 16370–16377.
48. Jenne, A., Hartig, J. S., Piganeau, N., Tauer, A., Samarsky, D. A., Green, M. R., Davies, J., and Famulok, M. (2001) *Nat. Biotechnol.* 19, 56–61.
49. Murray, J. B., Seyhan, A. A., Walter, N. G., Burke, J. M., and Scott, W. G. (1998) *Chem. Biol.* 5, 587–595.
50. Pinard, R., Lambert, D., Walter, N. G., Heckman, J. E., Major, F., and Burke, J. M. (1999) *Biochemistry* 38, 16035–16039.
51. Walter, N. G., Yang, N., and Burke, J. M. (2000) *J. Mol. Biol.* 298, 539–555.
52. Hampel, K. J., Walter, N. G., and Burke, J. M. (1998) *Biochemistry* 37, 14672–14682.
53. Mathews, D. H., Sabina, J., Zuker, M., and Turner, D. H. (1999) *J. Mol. Biol.* 288, 911–940.
54. Walter, N. G., and Burke, J. M. (1997) *RNA* 3, 392–404.
55. Esteban, J. A., Banerjee, A. R., and Burke, J. M. (1997) *J. Biol. Chem.* 272, 13629–13639.
56. Qin, P. Z., and Pyle, A. M. (1999) *Methods* 18, 60–70.
57. Konarska, M. M. (1999) *Methods* 18, 22–28.
58. Moore, M. J. (1999) *Methods Mol. Biol.* 118, 11–19.
59. Zhuang, X., Bartley, L. E., Babcock, H. P., Russell, R., Ha, T., Herschlag, D., and Chu, S. (2000) *Science* 288, 2048–2051.
60. Marcus, R. A. (1964) *Annu. Rev. Phys. Chem.* 15, 155.
61. Seidel, C. A. M., Schulz, A., and Sauer, M. H. M. (1996) *J. Phys. Chem.* 100, 5541–5553.
62. Dapprich, J., Walter, N. G., Salingue, F., and Staerk, H. (1997) *J. Fluor.* 7, 87S–89S.
63. Widengren, J., Dapprich, J., and Rigler, R. (1997) *Chem. Phys.* 216, 417–426.
64. Norman, D. G., Grainger, R. J., Uhrin, D., and Lilley, D. M. (2000) *Biochemistry* 39, 6317–6324.
65. Scaringe, S. A. (2000) *Methods Enzymol.* 317, 3–18.
66. Chowrira, B. M., Berzal-Herranz, A., and Burke, J. M. (1993) *Biochemistry* 32, 1088–1095.
67. Emerick, V. L., and Woodson, S. A. (1994) *Proc. Natl. Acad. Sci. USA* 91, 9675–9679.
68. Pan, J., Deras, M. L., and Woodson, S. A. (2000) *J. Mol. Biol.* 296, 133–144.
69. Bassi, G. S., Murchie, A. I., and Lilley, D. M. (1996) *RNA* 2, 756–768.
70. Esteban, J. A., Walter, N. G., Kotzorek, G., Heckman, J. E., and Burke, J. M. (1998) *Proc. Natl. Acad. Sci. USA* 95, 6091–6096.
71. Pinard, R., Heckman, J. E., and Burke, J. M. (1999) *J. Mol. Biol.* 287, 239–251.
72. Walter, N. G., Albinson, E., and Burke, J. M. (1997) *Nucleic Acids Symp. Ser.* 36, 175–177.
73. Song, L., Varma, C. A. G. O., Verhoeven, J. W., and Tanke, H. J. (1996) *Biophys. J.* 70, 2959–2968.
74. Chowrira, B. M., Berzal-Herranz, A., and Burke, J. M. (1991) *Nature* 354, 320–322.
75. Walter, N. G., Chan, P. A., Hampel, K. J., Millar, D. P., and Burke, J. M. (2001) *Biochemistry,* in press.
76. Haas, E., Wilchek, M., Katchalski-Katzir, E., and Steinberg, I. Z. (1975) *Proc. Natl. Acad. Sci. USA* 72, 1807–1811.
77. Miick, S. M., Fee, R. S., Millar, D. P., and Chazin, W. J. (1997) *Proc. Natl. Acad. Sci. USA* 94, 9080–9084.
78. Weiss, S. (2000) *Nat. Struct. Biol.* 7, 724–729.
79. Perkins, T. T., Smith, D. E., and Chu, S. (1997) *Science* 276, 2016–2021.
80. Schwille, P., Oehlenschlager, F., and Walter, N. G. (1996) *Biochemistry* 35, 10182–10193.
81. Ha, T., Ting, A. Y., Liang, J., Caldwell, W. B., Deniz, A. A., Chemla, D. S., Schultz, P. G., and Weiss, S. (1999) *Proc. Natl. Acad. Sci. USA* 96, 893–898.
82. Deniz, A. A., Laurence, T. A., Beligere, G. S., Dahan, M., Martin, A. B., Chemla, D. S., Dawson, P. E., Schultz, P. G., and Weiss, S. (2000) *Proc. Natl. Acad. Sci. USA* 97, 5179–5184.
83. Bevilacqua, P. C., Kierzek, R., Johnson, K. A., and Turner, D. H. (1992) *Science* 258, 1355–1358.